Wind load characteristics of single column three-sided billboards on sloping terrain

Yu Zhang, Qi Yuan, Wei He*

School of Mechanical and Electrical Engineering, Kunming University of Technology, Kunming, Yunnan, 650500, China.

*Corresponding author's e-mail: hw_big@126.com

Abstract. Considering the acceleration effect of sloping terrain on wind field, the wind load characteristics of single column three-sided billboard under sloping terrain are studied based on CFD numerical simulation and fluid-solid coupling method. Firstly, the flow field and surface wind pressure characteristics of the billboard at different slopes α, slope top position x and wind angle θ were discussed, then the load increase factor I_C was proposed as a quantitative indicator of wind damage, and finally wind resistant installation suggestions were given. The results show that the numerical calculations can be used for load characteristic studies. As α increases, the positive pressure extremes in panel 1-A gradually increase, and the reattachment capacity of the separated airflow in panels 2-A and 3-A decreases, resulting in an enhanced net wind pressure superposition effect on the panels. And the studied α in 45° has the most significant effect on load increase, therefore three types of wind resistance zoning are proposed, billboard installation should avoid class I ($0 \leq x < 1H$), where $I_C > 1.7$. In addition θ=60° can reduce panel skin damage and overall instability probability, θ=30° should be avoided to reduce support structure buckling damage.

Keywords: Sloping Terrain; Billboard; Wind Load Characteristics; Load Increase Factor; Wind Resistance Zoning

1 Introduction

Single column three-sided billboards are important carriers of outdoor communication media, and strong wind loads will lead to panel skin tearing, support structure buckling, and even overall collapse [1]. Therefore, it is important to carry out research on the wind load characteristics of billboards to ensure the safety of people's lives and property.

The Technical Specification for Outdoor Advertising Facilities in China [2] only gives the wind pressure coefficient of the billboard as a whole, which may lead to a discrepancy between the local design and the real situation, and the research on the wind load of single-column multi-faceted billboards needs to be further improved urgently. Early studies on the wind load characteristics of outdoor billboards were mainly focused on wind tunnel tests [3-4]. Using field tests and wind tunnel test

Z. Ahmad et al. (eds.), *Proceedings of the 2023 5th International Conference on Structural Seismic and Civil Engineering Research (ICSSCER 2023)*, Atlantis Highlights in Engineering 24,
https://doi.org/10.2991/978-94-6463-312-2_15

methods, Zuo et al. [5] and Wang [6] have shown that the structural form and wind angle of the panels have a significant effect on their wind loads. Wang, Hai et al. [7] gave theoretical calculations of the downwind and torsional wind vibration response of billboards. However, Smith et al. [8] evaluated the difference in results between full-scale field tests and wind tunnel scale down test methods, indicating that the average force coefficients obtained from wind tunnel tests were on the high side. Therefore, a large number of scholars used numerical simulation methods. Qin et al. [9] and Yang et al. [10] used computational fluid dynamics (CFD) methods for full-scale static wind load analysis of billboards to verify the feasibility of numerical simulation.

However, the experimental environment for wind tunnel experiments and numerical simulations has been limited to open and flat areas, ignoring the complex and variable wind fields caused by the undulating terrain. In addition to urban areas, sloping terrain is a typical landform in suburban areas. Lun et al. [11], Fang [12] and Zheng et al. have successively studied the two-dimensional and three-dimensional terrain wind fields of different slopes through wind tunnel tests and numerical simulations, and their studies have shown that the wind field characteristics are very different from those based on uniform rough planes, and different wind field acceleration effects exist for slopes of different slopes. The acceleration effect of wind farms will cause great potential danger to billboards installed in sloping terrain. The current research on the wind load characteristics of buildings in sloping terrain is focused on wind farms [14-15] and transmission towers [16-17], but the research on the wind load characteristics of billboards affected by terrain has not been carried out.

In summary, considering the acceleration effect of sloping terrain, the authors selected a single column three-sided billboard as the research object, and studied its wind load characteristics under sloping terrain through CFD numerical simulation and fluid-structure coupling method to provide reference for wind load calculation and wind hazard risk assessment of large billboard structures.

2 CFD calculation method

2.1 Research model

As shown in Figure 1, the section of the slope is shown in the schematic diagram, according to the slope grading, the slope α is selected as 0°, 15°, 30°, 45°, the slope height is H=50m, the slope length is L_1, the slope top length is L_2=8H, and the slope top platform size is $L_2 \times H$. A representative single column, three-sided type billboard (G3-6×18) was selected as the research model according to the Technical Specification for Outdoor Advertising Facilities in China. The billboard column is a cylindrical steel tube. The structural elevation, plan view and wind angle definition are shown in Figure 2. The structural dimensions of the billboard are shown in Table 1.

Table 1. Dimensions of the billboard model structure.

Model	*b*(m)	*c* (m)	*t*(m)	γ(°)	*h*(m)
G3-6×18	18	6	0.1	60	21

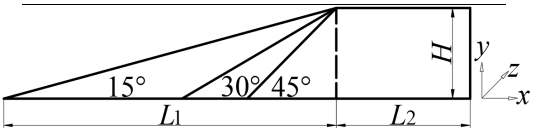

Fig. 1. Topographic profile of the slope.

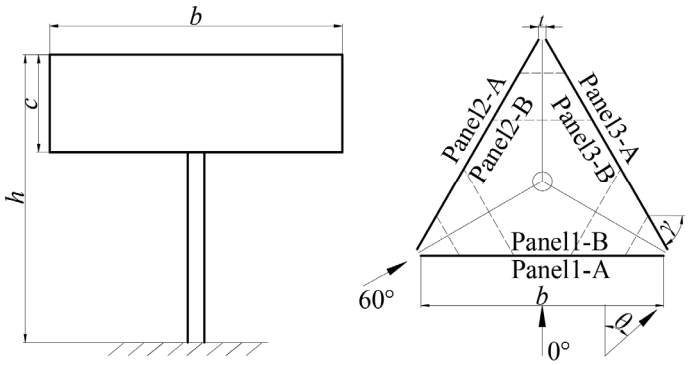

Fig. 2. Schematic diagram of the billboard structure and definition of the wind angle.

2.2 Calculation settings

Figure 3 shows the numerical calculation domain and boundary conditions. The dimensions are 15*H* × 5H × 8H and the obstruction rate is less than 3%. The centre of the column is at distance *x* from the gable in sloping terrain. Figure 4 shows the grid division, using interface to divide the flow field, the outer flow field uses a block structured grid, the inner flow field uses an unstructured grid, the billboard model adds a boundary layer grid, controlling the first layer grid y^+=30, the grid cell size around the slope refers to the literature [14], the minimum grid size is 1m, the grid growth rate is 1.1, and the standard wall function is chosen near the ground.

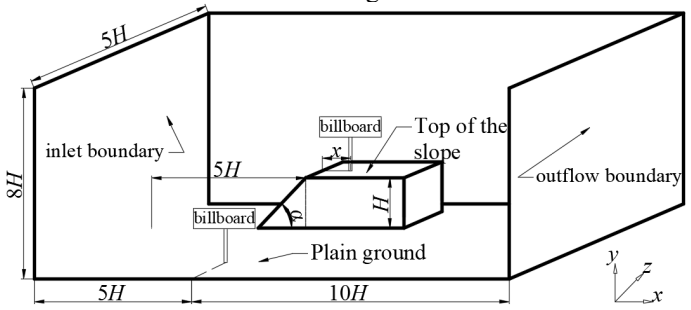

Fig. 3. Schematic diagram of the calculation domain.

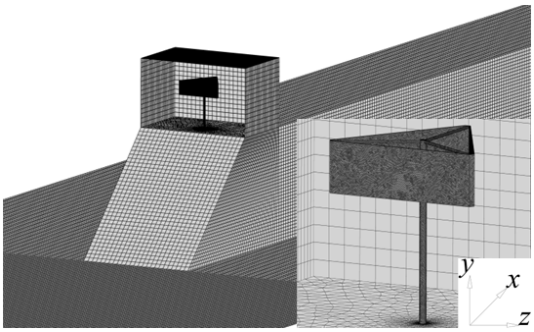

Fig. 4. Schematic diagram of the grid.

The inlet boundary is the velocity-inlet boundary and the wind profile is defined by a user-defined function (UDF) as a function of equation (1) (2).

$$V_Z = V_{10}(\frac{Z}{10})^{\alpha} \tag{1}$$

$$I_Z(Z) = I_{10}(\frac{Z}{10})^{-\alpha} \tag{2}$$

Where V_Z is the horizontal wind speed at Z; Z is the height from the ground; α is the ground roughness index for Class B landscapes, taken as 0.15; V_{10} is average wind speed at Z=10 m, chosen as a class 8 wind speed of 20.7m/s; I_{10}=0.14 is the nominal turbulence intensity at Z=10 m.

The outflow boundary is the pressure outlet; the ground and billboard surfaces are non-slip walls; the top and sides of the computational domain are symmetrical walls. The solution is based on the pressure solver and SIMPLEC algorithm; momentum and turbulent kinetic energy, turbulent kinetic energy dissipation rate and Reynolds stress discretization are in second order windward format; convergence accuracy is 10^{-5}.

2.3 Computational Fluid Dynamics (CFD) control equations

Zheng et al[13]. compare the simulation accuracy of the Standard *k-ε*, RNG *k-ε* and Realizable *k-ε* turbulence models and shows that the results of the Realizable *k-ε* turbulence model is closer to the wind tunnel tests, so the Realizable k-ε turbulence model is choose in this paper. Based on the Reynolds time-averaged method, Newton's second law and continuous medium theory, the controlling equations for viscous incompressible fluids are established as (3)(4), and the turbulent kinetic energy and dissipation rate transport equations are shown in the literature [14]:

$$\frac{\partial \overline{u_i}}{\partial x_i} = 0 \tag{3}$$

$$\frac{\partial \overline{u_i}}{\partial t} + \overline{u_i} \frac{\partial \overline{u_i}}{\partial x_j} = \overline{f_i} - \frac{1}{\rho} \frac{\partial \overline{p}}{\partial x_i} + \frac{\partial}{\partial x_j} (\upsilon \frac{\partial \overline{u_i}}{\partial x_j} - \overline{u_i' u_j'}) \tag{4}$$

where: ρ is the fluid density constant; p is the pressure; υ is the fluid kinematic viscosity constant; $\overline{u_i}$ is the time-averaged velocity component, $\overline{f_i}$ is the time-averaged external force per unit volume of fluid, $\overline{p}$ is the time-averaged pressure, and $\overline{u_i' u_j'}$ is the time-averaged resulting higher order term.

2.4 Model validation

To quantify the wind load characteristics of the billboard, the modal vibration diagram of the first three orders of the billboard is considered and the dimensionless wind load coefficients are defined: overall x-directional wind coefficient C_{Fx}, base x-directional shear coefficient C_{Vx}, base z-axis bending moment coefficient C_{Mz}, base torque coefficient C_{Tr}.

$$C_{Fx} = \frac{F_x}{0.5 \rho V_{ref}{}^2 bc} \tag{5}$$

$$C_{Vx} = \frac{V_x}{0.5 \rho V_{ref}{}^2 bc} \tag{6}$$

$$C_{Mz} = \frac{M_z}{0.5 \rho V_{ref}{}^2 bHc} \tag{7}$$

$$C_{Tr} = \frac{T}{0.5 \rho V_{ref}{}^2 b^2 c} \tag{8}$$

Where: F_x is the overall wind loads in x directions; T is the overall torque; V_x is the base shear forces in x directions; M_z is the base moments around the z axes; T is the base torque around the centre of the column; V_{ref} is the reference wind speed.

This section verifies the validity of CFD calculations through wind tunnel tests This section needs to verify the validity of CFD calculations. The experimental results of the G3-6×18 billboard in plain terrain are used as the validation object. The wind tunnel pressure measurement model is shown in Figure 5. The finite element model is successfully fitted with the first three orders of modal frequencies of the prototype, and the modal vibration patterns are the same, so that the calculated model has similar dynamic characteristics to the prototype.

The finite element analysis based on the fluid-structure coupling method was carried out to obtain the wind load coefficients of the billboard under different wind angles. The variation pattern of wind load coefficients of the billboard with wind direction

angle is shown in Figure 6. It can be found that the wind tunnel test and numerical simulation of each overall average wind force coefficient and the distribution law of the base reaction force coefficient with the wind direction angle are similar.

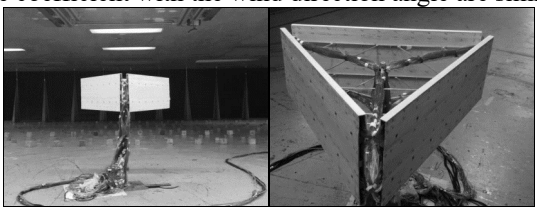

Fig. 5. Schematic diagram of the experimental model.

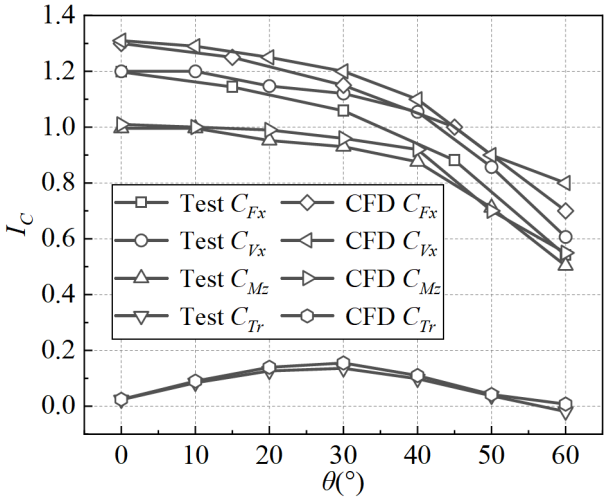

Fig. 6. Comparison of wind tunnel experiments and CFD calculations.

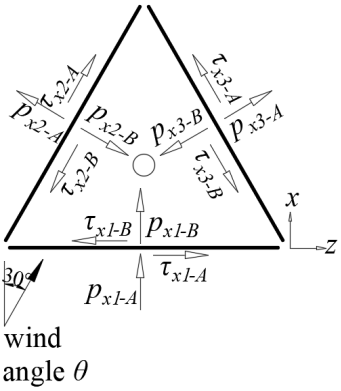

Fig. 7. Diagram of wind load loading on a three-sided billboard.

Figure 6 shows the comparison between the wind tunnel test and CFD calculation results, and the CFD simulation results are slightly larger than the wind tunnel test results. The maximum errors of C_{Fx}, C_{Vx}, C_{Mz}, and C_{Tr} are 8.1%, 7.6%, 2.2%, and 3.4%, respectively, which are within the controllable range (less than 15%). Figure 7 shows the wind load loading of the panels. As the pressure measurement data for the enclosure structure should be taken as the pressure difference between panels A and B as the net wind pressure. The experiments were conducted with a large number of wires arranged inside, which prevented the separated vortices from entering the inner layer, making the negative pressure in the inner layer reduced. And when solving based on computational fluid dynamics, as air is viscous, there is a surface viscous force τ_i at each surface of the billboard in addition to the positive pressure p_i, which is in the same direction as the airflow. Therefore, the load obtained by CFD simulation is slightly higher than the load obtained from the wind tunnel test.

3 Load characteristics of billboards in sloping terrain

The wind angle θ=0° is chosen. According to the study the acceleration effect is most pronounced near the eaves of the slope, and to reserve the installation site for the three-sided billboard, the centre of the column is installed to x=10m.

3.1 Flow field analysis

Figure 8 shows the flow and velocity distribution clouds around the billboard at different slopes. The cross-section is taken downwind of the vertical section of the billboard and the middle cross-section of the panel. The panel is a blunt body structure and the airflow separates at the angles to create separation vortices, with the flow phenomenon of airflow separation, vortex impact and vortex reattachment. Before the foot of the slope, the velocity contour increases with height, when it reaches the slope the contour rises and gradually rises with the increase in slope. The wind velocity continues to increase as the flow hits the billboard, reaching a maximum velocity at the top of the billboard, with the wake becoming more turbulent as the gradient increases. The airflow stagnation point in panel 1-A gradually shifts downwards due to the lifting effect of the airflow with increasing slope. The internal vortex becomes progressively more turbulent due to the disturbance of the vertical component of the wind speed. Due to the sharp increase in the incoming Reynolds number, the inverse pressure gradient of the separating airflow decreases and the re-attachment behaviour of the vortices in the outer panels 2-A and 3-A gradually decreases. Until at a slope of 45°, no significant vortices are found and the separated airflow converges directly into the wake.

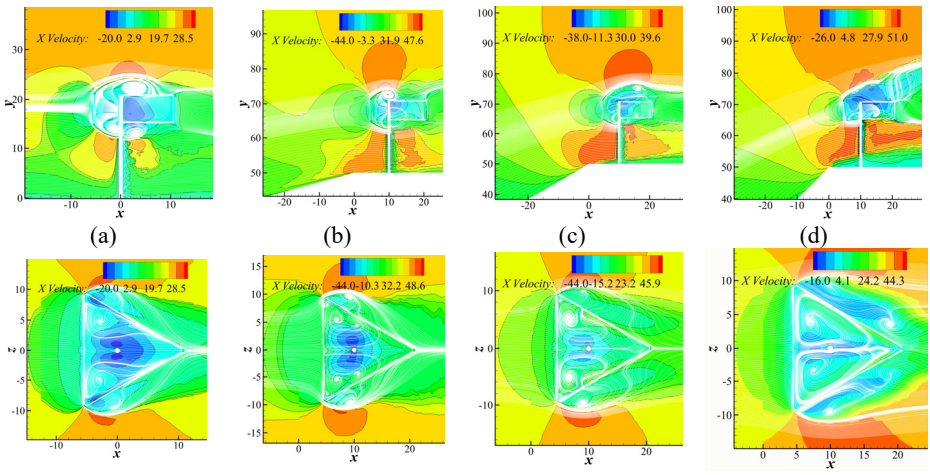

Fig. 8. Flow and velocity clouds for billboards at different slopes: (a) Vertical section at α=0°; (b) Vertical section at α=15°; (c) Vertical section at α=30°; (d) Vertical section at α=45°; (e) Middle Cross-section at α=0°; (f) Middle Cross-section at α=15°; (g) Middle Cross-section at α=30°; (h) Middle Cross-section at α=45°.

3.2 Surface wind pressure distribution characteristics

Defines the dimensionless average wind pressure coefficient on the surface of a building:

$$C_{pi} = \frac{P_i}{0.5\rho V_{ref}^{\ 2}} \tag{9}$$

Where C_{Pi} is the wind pressure coefficient at the measurement point; P_i is the wind pressure at the measurement point; ρ is the air density; V_{ref} is the wind speed at the reference height

Figure 9 shows a cloud plot of the average wind pressure distribution for the panels at the most unfavourable wind angle of 0°. The wind pressure distribution of the panels is symmetrically distributed. This causes the horizontal component of wind speed to increase with increasing slope, resulting in a gradual increase in the extreme value of the windward panel wind pressure coefficient. The airflow stagnation point gradually shifts downwards with increasing slope, leading to a gradual shift in the location of the maximum wind pressure. As the separation vortex impinges on the inner surfaces of panels 2 and 3, this results in positive and negative pressures in panels 2-B and 3-B. And as the slope increases, the upper and lower separated vortices hit the inner surface directly, resulting in an increase in both the positive pressure value and range. As the re-attachment behaviour of the separated vortices weakens with increasing slope, negative pressures are formed in all of panels 2-B and 3-B, and the total pressure increases at the intersection of panels 2-B and 3-B. Therefore, when designing the

structure, the superimposed effect of positive and negative pressures on the inner and outer surfaces of the panels should be considered.

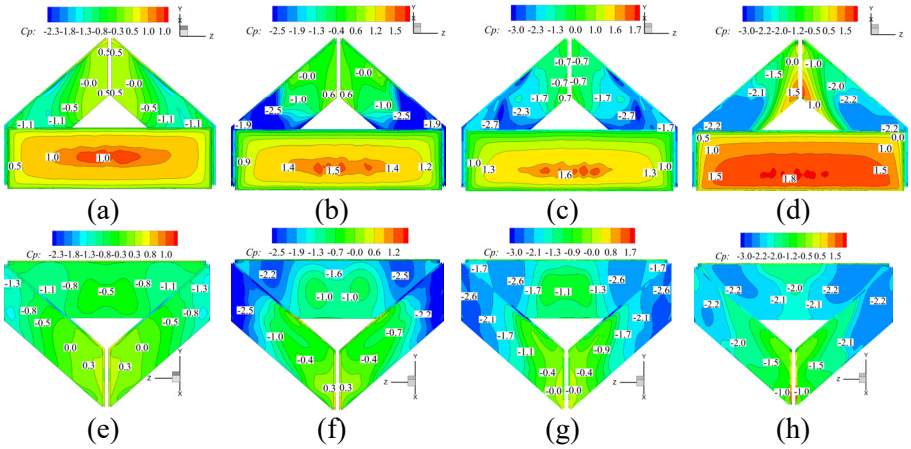

Fig. 9. Wind pressure coefficients on billboard surfaces at different slopes: (a) Direction of incoming flow at α=0°; (b) Direction of incoming flow at α=15°; (c) Direction of incoming flow at α=30°; (d) Direction of incoming flow at α=45°; (e) Leeward direction at α=0°; (f) Leeward direction at α=15°; (g) Leeward direction at α=30°; (h) Leeward direction at α=40°.

4 Recommendations for wind resistant installation of billboards on sloping terrain

The wind risk factor R is commonly used to measure the degree of risk of a billboard under wind loads, with R defined as the ratio of a quantitative indicator of a certain form of damage to the corresponding threshold value. When the billboard is installed on sloping terrain, subject to the acceleration effect of the wind field, the risk factor should be multiplied by the corresponding correction factor, i.e. the load increase factor. Define the load increase factor I_C:

$$I_C = \frac{I_{C,s}}{I_{C,f}} \tag{10}$$

where the subscript C indicates the wind load factor category and the subscripts s and f indicate the load factors for slopes and plains respectively.

The wind damage modes of the outdoor large single column billboard shown in Figure 10 are divided into three main categories: (a) panel skin tear (b) support structure buckling (c) overall overturning. The most dangerous slope for billboard wind effects from the previous chapter study is 45°. This section integrates the billboard wind damage modes and each response index, using IFx, ITr, IVx and IMz as quantitative indicators of wind resistance, corresponding to damage modes (a) (b) (c) respectively.

(a) (b) (c)

Fig. 10. Typical damage pattern of a single column billboard.

Table 2. Billboard load increase factor IC for α=45° sloping terrain.

x, θ	I_{Fx}	I_{Vx}	I_{Tr}	I_{Mz}	x, θ	I_{Fx}	I_{Vx}	I_{Tr}	I_{Mz}
x=0.2H, θ=0°	2.446	3.082	2.622	2.711	x=0.2H, θ=10°	2.379	2.949	2.822	2.689
x=0.4H, θ=0°	1.623	2.311	1.991	2.230	x=0.2H, θ=20°	2.361	2.827	3.163	2.601
x=1H, θ=0°	1.498	1.552	1.765	1.696	x=0.2H, θ=30°	2.357	2.758	3.446	2.553
x=2H, θ=0°	1.304	1.494	1.512	1.481	x=0.2H, θ=40°	2.165	2.391	3.238	2.367
x=3H, θ=0°	1.089	1.267	1.217	1.246	x=0.2H, θ=50°	1.778	1.981	2.981	2.136
x=4H, θ=0°	1.112	1.272	1.218	1.255	x=0.2H, θ=60°	1.436	1.472	2.512	1.701
x=5H, θ=0°	1.098	1.271	1.215	1.242					
x=6H, θ=0°	1.112	1.272	1.218	1.248					
x=8H, θ=0°	1.112	1.267	1.212	1.246					

Table 2 gives the law of variation of each response indicator IC with respect to the installation position x at the top of the slope for the most unfavourable slope 45° of the slope studied in this paper, and also gives the law of variation of each response indicator with respect to the wind angle at the gable position at the top of the slope. The wind risk factor R takes the maximum value for multiple damage patterns that exist simultaneously. Therefore the expression for the load increase factor of the billboard is defined:

$$I_C = \max(I_{Fx}, I_{Tr}, I_{Vx}, I_{Mz}) \tag{11}$$

Figure 11 divides the slope tops into three types of installation areas: (I) class 1 is the area of significantly increasing response (0≤x<1H), where IC>1.7; (II) class 2 is the area of diminishing response (1H≤x<4H), where 1.2≤IC<1.7; (III) class 3 is the area of insignificant increasing response (x ≥ 4H), where IC is around 1.2.

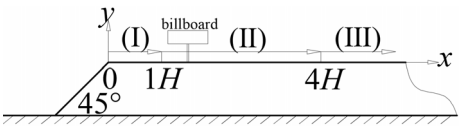

Fig. 11. Diagram of wind resistant installation zoning on sloping land.

5 Conclusion

In this paper, based on CFD numerical calculation method and fluid-structure coupled finite element method, the load characteristics of single column three-sided billboard under sloping terrain are studied, and the main conclusions are as follows:

(1) The results of the numerical calculations are similar to those of the wind tunnel tests in plain terrain, and the distribution patterns of the overall average wind coefficients and the basal reaction coefficients with wind angle are similar, indicating the feasibility of the numerical calculation method.

(2) As the slope increases, the acceleration effect of the wind field gradually increases. The wind speed contour gradually rises causing the height of the airflow stagnation point in panel 1-A to decrease, resulting in a gradual increase in the extreme value of the positive pressure in panel 1-A and a downward shift in position height. The re-attachment of separated airflow in panels 2-A and 3-A is weakened, which increases the net wind pressure superposition effect in panels. The superimposed effect of the wind pressure in the backwind panel should be taken into account in the structural design.

(3) A load increase factor IC is proposed, which increases with slope, with the most significant effect of load increase at 45° slope among the slopes studied. Using IC as a quantitative indicator of wind damage, and for the most unfavourable slopes, the following wind resistance zones are proposed: (I) class 1 is the area of significantly increasing response ($0 \leq x < 1H$), where $I_C > 1.7$; (II) class 2 is the area of diminishing response ($1H \leq x < 4H$), where $1.2 \leq I_C < 1.7$; (III) class 3 is the area of insignificant increasing response ($x \geq 4H$), where I_C is around 1.2. The installation site should be sited to avoid sloping gable locations, i.e. class 1. In addition, a wind angle of $\theta = 60°$ reduces the potential for panel skin damage and overall destabilisation overturning. Wind angle $\theta = 30°$ should be avoided to reduce buckling damage to the supporting structure.

Acknowledgments

The full authors acknowledge funding from the National Natural Science Foundation of China under Grant No. 51168020.

References

1. Wen J Y and Xie Q 2020 Field investigation and structural analysis of wind-induced collapse of outdoor single-post billboards *Engineering Failure Analysis*. **117**.

2. *Load Code for the Design of Building Structures* (GB 50009-2012) (Beijing: China-Architecture and Building Press)
3. Letchford C W, Homels J D 1994 Wind loads on free-standing walls in turbulent boundary layers *Journal of Wind Engineering and Industrial Aerodynamics*. **51:** 1-27
4. Letchford C W 2001 Wind loads on rectangular signboards and hoardings *Journal of Wind Engineering and Industrial Aerodynamics*. **89:** 135-151
5. Zuo D L, Smith D A and Mehta K C 2014 Experimental study of wind loading of rectangular sign structures *Journal of Wind Engineering and Industrial Aerodynamics*,**130:**62-74
6. Wang D H，Chen X ZH，Li J，et al 2016 Wind load characteristics of large billboard structures with two-plate and three-plate configurations *Wind and Structures*,**22(6):**703.
7. Wang D H, Li ZH H and Li J 2018 Experimental study on wind loading of large outdoor single column three-sided billboards (in Chinese) *Journal of Civil Engineering*,**51(08)**
8. Smith D A, Zuo D L and Mehta K C 2014 Characteristics of wind induced net force and torque on a rectangular sign measured in the field *Journal of Wind Engineering and Industrial Aerodynamics*, **133:**80-91
9. Qin Y, Zhang Y C, Wang CH G 2004 Feasibility study of numerical wind tunnel for simulating static wind loads on structures (in Chinese) *Journal of Harbin Institute of Technology* **12:**1593-97.
10. Yang W W, Luo J C and Du Y N 2022 Pneumatic optimization of wind resistance of outdoor large three-sided single column billboards (in Chinese) *Journal of Lanzhou University of Technology*, **48(01):**143-9.
11. Lun Y F, Mochida A，Yoshino H, et al 2007Applicability of linear type revised k-e models to flow over topo-graphic features *Journal of Wind Engineering and Industrial Aerodynamics*,**95(5):**371-84.
12. Fang P Z，Zheng D Q，Li L，et al 2019 Numerical and experimental study of the aerodynamic characteristics around two-dimensional terrain with different slope angles(in Chinese) *Frontiers of Earth Science* ,**13(4):**705-20.
13. Zheng D Q, Li L, Fang P Z and Ma W Y 2021 Study on numerical simulation methods for wind fields on steep mountain slopes (in Chinese) *Journal of Computational Mechanic*,**38(05):**644-50.
14. Zuo W, Li H M, Rui X M, Wang X D and Kang SH 2019 Numerical simulation study of hillside topography of wind farms (in Chinese) *Journal of Solar Energy*,**40(05):**1441-47.
15. Niu J G, Chen X and Yan L 2016 Numerical simulation of wind pressure of wind turbine tower structure on sloping ground (in Chinese) *Journal of Civil Engineering and Management*,**33(06):**6-11.
16. Yao J F, Shen G H, Lou W J, Guo Y and Xing Y L 2017 Wind field characteristics of three-dimensional hills and the influence on the wind-induced response of transmission towers (in Chinese) *Vibration and Impact*,**36(18):**78-84.
17. Liu M L, Lv H K, Luo K, Wang M J, Fan J R and Chi W 2020 Numerical simulation of wind-induced response of power transmission tower system under realistic mountainous terrain conditions (in Chinese) *Vibration and shock*,**39(24):**232-239.